JGR Atmospheres

RESEARCH ARTICLE
10.1029/2022JD036965

Microphysical Pathways Active Within Thunderstorms and Their Sensitivity to CCN Concentration and Wind Shear

Andrew I. Barrett[1] **and Corinna Hoose**[1]

[1]Institute for Meteorology and Climate Research, Karlsruhe Institute of Technology, Karlsruhe, Germany

Key Points:

- Microphysical pathways are constructed by tracking microphysical processes rates and closing the hydrometeor mass budget
- More cloud condensation nuclei lead to less surface precipitation and hail, due to smaller cloud drop sizes and reduced riming collection efficiency
- Simulations with constant riming collection efficiency reveal two different hail formation pathways

Correspondence to:

A. I. Barrett and C. Hoose,
andrew.barrett@kit.edu;
corinna.hoose@kit.edu

Citation:

Barrett, A. I., & Hoose, C. (2023). Microphysical pathways active within thunderstorms and their sensitivity to CCN concentration and wind shear. *Journal of Geophysical Research: Atmospheres*, *128*, e2022JD036965. https://doi.org/10.1029/2022JD036965

Received 7 MAY 2022
Accepted 4 FEB 2023

Author Contributions:

Conceptualization: Andrew I. Barrett, Corinna Hoose
Formal analysis: Andrew I. Barrett
Funding acquisition: Andrew I. Barrett, Corinna Hoose
Investigation: Andrew I. Barrett
Methodology: Andrew I. Barrett, Corinna Hoose
Software: Andrew I. Barrett
Visualization: Andrew I. Barrett
Writing – original draft: Andrew I. Barrett
Writing – review & editing: Andrew I. Barrett, Corinna Hoose

Abstract The impact of cloud condensation nuclei (CCN) concentration on microphysical processes within thunderstorms and the resulting surface precipitation is not fully understood yet. In this work, an analysis of the microphysical pathways occurring in these clouds is proposed to systematically investigate and understand these sensitivities. Thunderstorms were simulated using convection-permitting (1 km horizontal grid spacing) idealized simulations with the ICON model, which included a 2-moment microphysics parameterization. Cloud condensation nuclei concentrations were increased from 100 to 3,200 CCN/cm^3, in five different wind shear environments ranging from 18 to 50 m/s. Large and systematic decreases of surface precipitation (up to 35%) and hail (up to 90%) were found as CCN was increased. Wind shear changes the details, but not the sign, of the sensitivity to CCN. The microphysical process rates were tracked throughout each simulation, closing the mass budget for each hydrometeor class, and collected together into "microphysical pathways," which quantify the different growth processes leading to surface precipitation. Almost all surface precipitation occurred through the mixed-phase pathway, where graupel and hail grow by riming and later melt as they fall to the surface. The mixed-phase pathway is sensitive to CCN concentration changes as a result of changes to the riming rate, which were systematically evaluated. Supercooled water content was almost insensitive to increasing CCN concentration, but decreased cloud drop size led to a large reduction in the riming efficiency (from 0.79 to 0.24) between supercooled cloud drops and graupel or hail, resulting in less surface precipitation.

Plain Language Summary The amount of rain and hail from thunderstorms can be influenced by the amount of pollution in the form of aerosol particles, which determine how many cloud droplets form and how large they are. Unfortunately, different numerical models give different answers on whether rain and hail increase or decrease if pollution increases. In this article, we present a new analysis method helping to identify the small-scale processes which are responsible for the increase or decrease in a specific numerical scheme. We apply it to simulations of thunderstorms and show that the decrease of rain and hail in the numerical model used here is mostly linked to the riming process. Riming is the collision of cloud droplets and frozen particles at temperatures below 0°C, such that the liquid water freezes to the surface of the ice particles and makes them bigger. Less riming occurs when pollution increases, because cloud droplets are smaller. This process is very important because nearly all rain reaching the surface consists of melted ice particles.

1. Introduction

Thunderstorms produce numerous weather hazards including lightning, strong winds and extreme precipitation. Precipitation rates above 100 mm/hr and hail larger than 5 cm is frequently reported from the most intense thunderstorms. The rain drops, hail stones and other precipitation hydrometeors are formed within thunderstorms as the result of various microphysical processes (such as growth by condensation, collisions with other hydrometeors, freezing and melting, among others). A chain of several microphysical processes is usually responsible for the formation of precipitating hydrometeors; several chains exist within convective storms although not all are necessarily active in any particular storm or at a particular time. We refer to these chains of microphysical processes as "microphysical pathways" throughout this paper.

The amount and type of surface precipitation produced within thunderstorms is sensitive to environmental conditions. Larger and more organized thunderstorms are more likely to form when the wind shear (often defined as vector difference between winds at 0 and 6 km) increases. Increased wind shear can increase the width of the storm updraft (Marion & Trapp, 2019; Warren et al., 2017), the storm lifetime and therefore the overall precipitation total. Furthermore, the interaction between low-level shear and cold pools is also connected to the formation of long-lived squall lines (Rotunno et al., 1988).

Similarly, the aerosol concentration in the atmosphere also affects the precipitation process by modifying the number and size of hydrometeors within clouds. The aerosols, by virtue of their ability to act as cloud condensation nuclei (CCN) or ice nucleating particles (INPs), affect the cloud properties and therefore microphysical processes. Increased CCN concentrations lead to more numerous but smaller cloud drops at cloud base. Increased INP concentrations lead to freezing at higher temperatures or faster glaciation. However, the overall impact of aerosols on convective precipitation remains uncertain (Tao et al., 2012). Neither observational nor modeling studies are currently able to provide a clear picture. Variability of CCN in observational studies cannot be fully separated from meteorological variability, which makes it impossible to attribute differences in cloud or precipitation quantities to changing CCN alone (Stevens & Feingold, 2009). Modeling studies allow for meteorological and CCN variables to be varied independently; however, results from different models, environments, days and timescales give almost every possible sensitivity to CCN concentration (Khain et al., 2008).

Recent increases in modeling and computational abilities have enabled CCN effects on convective clouds to be simulated at high resolution. The sensitivity of hail to increasing CCN concentration is particularly uncertain. Multiple studies show that hail amount can increase (Chen et al., 2019; Khain et al., 2011; Khain et al., 2015; Loftus & Cotton, 2014), or decrease (Barrett et al., 2019; Morrison, 2012; Noppel et al., 2010; Wellmann et al., 2018). Some of these studies also report non-monotonic sensitivities (e.g. Noppel et al., 2010) with increasing CCN concentration. Other studies show that the sensitivity depends on other factors. For example, Carrió et al. (2014) found a dependence on cloud base height, while Morrison (2012) found that the inclusion of an additional hail hydrometeor class changed the sign of the sensitivity, as did changing the assumed fall velocity of hail to that of snow. These studies used a variety of 2D or 3D simulations, different microphysical parameterizations of various complexity (2-moment, 3-moment, bin microphysics) and analyzed simulations of either idealized or real cases. These differences in CCN sensitivity likely result from the different assumptions within the microphysical parameterizations; however, we still lack convincing explanations for these diverse results.

One way to improve our understanding of these different sensitivities is to better understand the physical mechanisms through which precipitation is formed and how these mechanisms are affected by CCN concentration in different modeling setups. By understanding how each of the microphysical pathways is represented in each model and how sensitive they each are to CCN concentration in different situations could help us to disentangle their different sensitivities.

In this work, we analyze the sensitivity of surface precipitation to CCN concentration in idealized simulations of thunderstorms using the ICON model. We explore the potential that a deep analysis of the microphysical pathways can offer. Furthermore, we determine whether the sensitivity to CCN and important microphysical pathways remains constant as the wind shear is increased.

Details about the model, model setup and selected microphysical parameterizations are given in Section 2. Using the microphysical pathways outlined and quantified in Section 2.3, precipitation and hail statistics from the simulation are analyzed in Section 3. The causes of the sensitivities are discussed in Section 4. Section 5 contains discussion of the relevance of the work and conclusions are drawn in Section 6.

2. Model and Methods

2.1. Model Experimental Setup

A short three-dimensional idealized supercell-type simulation with the ICON model, version 2.6.2.2, is used for each setup. The model is initialized with the temperature and humidity profiles of Weisman and Klemp (1982) and westerly winds increasing with height from zero at the surface up to 6 km altitude. All fields are horizontally-homogeneous at initialization. Convection is initiated by the release of a 3 K warm bubble in the first timestep. The first 2 hr are simulated, during which dynamical feedbacks to the updraft are limited and are therefore comparable for all CCN concentrations. The idealized simulation is justified as we are interested mainly in in-cloud processes rather than the specifics of convective initiation.

To study the sensitivity of precipitation and hail formation to CCN concentration and wind shear, 20 simulations are run. Four values are chosen as representative for low, intermediate, high and very high CCN concentrations: 100, 500, 1,700, 3,200 CCN/cm^3 near the surface (Noppel et al., 2010); CCN are uniformly distributed in the horizontal, and decrease exponentially above 4 km with a scale height of 4 km. The initial horizontal winds are

Table 1
Details of the ICON Model Setup Used for This Study

Parameter	Value/reference
Model grid	
Horizontal resolution	1 km
Vertical levels	100
Domain	300 × 100 km^2 torus (double-periodic boundaries)
Model integration	
Timestep	3 s
Duration	2 hr
Environmental setup	
Thermodynamic profile	unstable (Weisman & Klemp, 1982)
Convection initiation	warm bubble (+3 K, 15 km radius)
Wind profile	westerly winds; linear increase to maximum speed (18–50 m/s), at and above 6 km
CCN concentration	100–3,200 CCN/cm^3, horizontally uniform, constant up to 4 km, exponential decrease above (Noppel et al., 2010)
Physics parameterizations	
Cloud microphysics	two-moment, six-category scheme (Blahak, 2008; Seifert & Beheng, 2006a)
CCN activation	Segal and Khain (2006)
Radiation	None
Ice nucleation	volume-dependent rain drop freezing (Bigg, 1953), immersion freezing of cloud droplets and deposition nucleation (Phillips et al., 2008)

purely westerly, increasing linearly from zero at the surface to u_{max} at and above 6 km altitude; u_{max} values of 18, 25, 32, 42, 50 m/s are used. Each simulation is 2 hr duration, and the sensitivities are evaluated at the end of this 2-hr period. Abbreviations of the form CCN100 are used to refer to all simulations with 100 CCN/cm^3; similarly WS18 refers to all simulations with 18 m/s wind shear. Specific simulations are referred to by combining these (e.g., WS18 + CCN100).

The model setup used for this study is summarized in Table 1. Specific details relevant for this study are explained in the following subsections.

2.2. Microphysics Parameterization

In this study, the 2-moment bulk microphysics scheme of Seifert and Beheng (2006a, 2006b), with the additional hail category (Blahak, 2008) is used. The main processes important for discussions within this paper are described here. For a more complete description of the parameterization scheme, readers are referred to the original papers.

2.2.1. Condensation

Condensation within ICON is performed before the call to the parameterized microphysics. This is performed through saturation adjustment, where any supersaturation produced through the model dynamics is removed and an appropriate amount of cloud water and latent heating is produced such that the grid box achieves 100% relative humidity. Similarly, cloud water is evaporated in sub-saturated environments. The use of saturation adjustment can potentially lead to higher updrafts (Grabowski & Morrison, 2017) and limit aerosol-convection interactions (Lebo et al., 2012; Zhang et al., 2021).

2.2.2. CCN Activation

The CCN activation uses the lookup tables by Segal and Khain (2006), which determine the number of activated cloud droplets based on vertical velocity. Activation of CCN occurs only where supersaturation with respect to liquid exists and grid-scale vertical velocity is positive (upward). However, it is the vertical velocity, rather than supersaturation, which is used to determine the number of CCN that are activated. Activation of CCN can occur

both at cloud base, and within the cloud at grid-boxes where supersaturation exists at the beginning of the cloud microphysics calculations. CCN concentrations used in this paper are 100, 500, 1,700, 3,200 CCN/cm^3, and are not depleted by droplet formation. These CCN concentrations are constant in the lowest 4 km but decrease exponentially with height above 4 km, with a scale height of 2 km.

2.2.3. Autoconversion and Accretion (Converting Cloud Water to Rain Water)

The autoconversion of cloud drops to rain, and the accretion of cloud drops by falling rains drops are parameterized following Seifert and Beheng (2001). The autoconversion rate approximately scales with $L_c^2 x_c^2$, where L_c is the cloud water content in kg/m^3 and x_c is the mean mass of cloud drops. The full equations are given by Seifert and Beheng (2006a, Equations 4–6) Accretion rate approximately scales with $L_c L_r$, where L_r is the rain water content in kg/m^3. The full equations are given by Seifert and Beheng (2006a, Equations 7, 8).

2.2.4. Rain Freezing

The freezing of rain drops is parameterized in two stages. First the freezing rate of rain drops is determined from the parameterization of Bigg (1953), depending on temperature and rain drop mean size. Second, the fraction of these frozen drops becoming snow, graupel or hail is determined by the size of rain drops within the gridbox. Rain drops with diameters below 500 μm become ice; between 500 and 1,250 μm become graupel and rain drops with diameter larger than 1,250 μm become hail. Heterogeneous and homogeneous freezing of cloud droplets as well as heterogeneous ice nucleation from the vapor phase are not relevant for the microphysical pathways leading to surface precipitation and are therefore not discussed here.

2.2.5. Graupel Formation

Graupel is either formed directly from rain freezing (see above) or from riming on to ice or snow. When the riming rate within a grid box exceeds the rate of growth by vapor deposition, the ice (or snow) becomes graupel. All mass and number at this grid point is moved from the ice (or snow) category to the graupel category.

2.2.6. Hail Formation

Hail is either formed directly from rain freezing (see above) or when riming onto graupel particles leads to "wet growth"; where latent heating of freezing increases the hydrometeor surface temperature above 0°C. Threshold sizes are determined in the model using lookup tables, based on temperature and liquid water content. The mass and number of graupel stones experiencing wet growth are moved to the hail category.

2.2.7. Riming

Riming can occur when a frozen hydrometeor collides with a liquid hydrometeor. The number of collisions is parameterized taking into account the full size distribution of both frozen and liquid hydrometeors and their respective fall velocities. Each collision type has an associated collection efficiency, based on particle types and mean sizes Seifert and Beheng (2006a). After all collisions are calculated, the mass and number of liquid hydrometeors which are collected are moved to the frozen category of the collector. In some cases, riming leads to a change of the frozen hydrometeor classification (see graupel formation and hail formation above).

2.3. Possible Pathways

To simplify the numerous interactions of microphysical processes inside the model, we attempt to reduce the complexity by grouping the processes into a number of possible microphysical pathways. Each pathway represents a possible path for hydrometeors to grow, freeze, melt and evaporate on their way to reaching the surface or, alternatively, remaining suspended in the atmosphere or returning to the vapor phase. The relative importance of each pathway is quantified for our simulations in Section 3.3. In the most simplified form, there are essentially four possible pathways that hydrometeors can follow.

1. *Warm-rain pathway*: Cloud water is produced through condensation. Cloud droplets grow through collision and coalescence, forming rain ("autoconversion" in model parameterizations). Rain droplets form before freezing occurs. Rain droplets fall through the cloud, collecting other cloud and rain drops ("accretion") as they fall. Rain drop fall from the cloud, begin to evaporate and may reach the surface.
2. *Mixed-phase pathway*: Convection reaches heights where the air is cold enough for freezing to begin (at least −4°C). Some supercooled water freezes. These frozen drops collide with and collect ("riming") supercooled

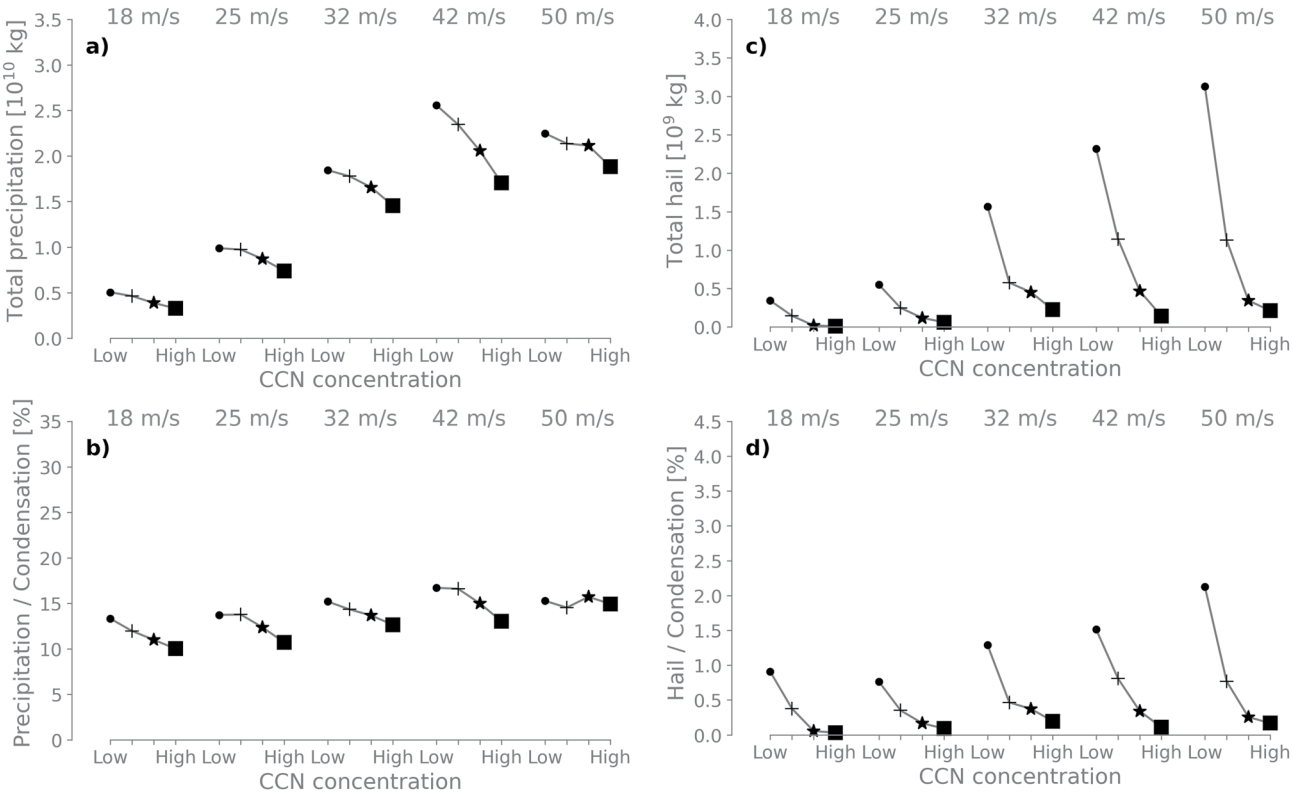

Figure 1. Accumulated precipitation (a) and surface hail fall (b) in each simulation. Wind shear is given above the plots, while the four symbols for each wind shear represent the four cloud condensation nuclei (CCN) cases (circle: 100, cross: 500, star: 1,700, square: 3,200 CCN/cm^3). The lower two plots show the precipitation efficiency for rain (c) and hail (d), by normalizing the quantities in the top row by the total condensation occurring within the simulation.

liquid drops (either cloud or rain), forming graupel and later hail. Graupel and hail fall to the melting level while continuing to collect mass by riming. Melting below the melting level begins to form rain; the unmelted parts of the frozen particles fall to the surface, as do the rain drops formed by melting (subject to evaporation).

3. *Ice-phase pathway*: Convection reaches heights where freezing occurs. No significant riming occurs, either because the freezing is so efficient that all water freezes or the liquid water content is sufficiently low. Vapor deposition allows the ice particles to grow and the liquid evaporates (Wegener-Bergeron-Findeisen process). Frozen particles (ice or snow) grow by colliding with and collecting other frozen particles ("aggregation") and/or by vapor deposition. Ice and snow particles fall to the melting level. Particle melting begins to form rain, or the frozen particles fall to the surface.
4. *Non-precipitating pathway*: particles follow pathway 2 or 3; however, the growth is sufficiently slow that the particles do not achieve fall velocities that (notably) exceeds the air vertical velocity and therefore neither grow nor fall. These hydrometeors remain lofted in the atmosphere (e.g., in a convective anvil) and eventually their mass returns to the vapor phase as evaporation or sublimation occurs.

3. Results

3.1. Precipitation and Hail Totals

Both the total precipitation (sum of rain and hail, as in the presented simulations the other frozen hydrometeors melt entirely before reaching the ground) and the hail mass reaching the surface are sensitive to both CCN concentration and wind shear (Figure 1). Precipitation systematically increases with increasing wind shear and hail generally increases with wind shear (in 82% of simulations pairs). Precipitation and hail both systematically decrease with increasing CCN concentration. The high-shear, low-CCN (WS42 + CCN100) simulation produces the most precipitation (domain average: 0.931 mm) whereas the low-shear, high-CCN (WS18 + CCN3200) simulation produces the least (0.068 mm). The explanation and reasons behind these differences are detailed in the following two sections.

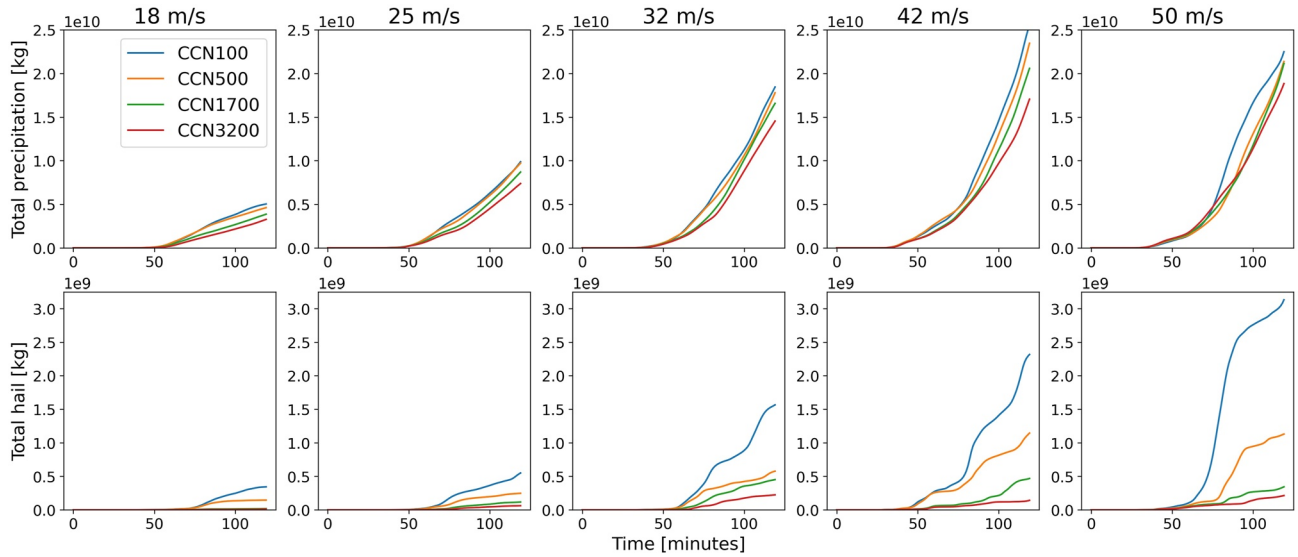

Figure 2. Timeseries of domain-integrated accumulated precipitation (top row) and total hail fall (bottom row).

The total surface precipitation increases steadily with time through the simulation, whereas the hail formation appears to cycle between active and less active periods, especially when wind shear is 32 m/s or above (Figure 2). Importantly, the ordering of simulations from low to high surface precipitation or surface hail is almost fully consistent throughout the 2-hr simulation period (Figure 2), meaning that the results are not dependent on this specific evaluation time. Similarly, the ordering of simulations based on precipitation and hail flux at a certain distance below cloud base is consistent (not shown), indicating that analysis of these simulations after 2 hr and at the surface is robust and representative of the simulations on the whole.

3.2. 2D Structure of Convective Cells

The vertical and horizontal structure of hydrometeors within the convective cells, and the process leading to addition or removal of mass from each hydrometeor category were created through compositing. An example for the WS18 + CCN100 simulation (Figure 3) highlights the major source and sink regions of hydrometeor mass for the different microphysical pathways.

Rain is produced within the updraft core (Figure 3a), through collision and coalescence of cloud droplets (model processes: autoconversion and accretion). Between 6 and 9 km altitude these rain drops begin to freeze (rain freezing) and then are collected by frozen hydrometeors (riming). This freezing and riming means that no rain mass is transported above 9 km altitude and happens before the rain drops leave the updraft and fall toward the ground. The importance of the freezing and riming processes mean the warm-rain pathway is almost inactive, but that the precipitation is produced via the mixed-phase pathway. Rain mass is formed in the mixed-phase pathway through melting of graupel and hail, starting just below 4 km altitude. Due to the non-instantaneous melting of large ice particles and the sequential operator splitting within ICON, it can happen that there is a sink of rain due to riming and a source of rain due to melting at the same pixel within one timestep. This artificial cycling of mass between rain and rimed particles near the melting level is omitted from the mass budgets.

Graupel is initially formed by freezing of rain drops (Figure 3b), of through conversion of ice and snow to graupel as they begin to rime. However, most of the mass is formed by riming within the updraft core above 7 km and much of the mass remains suspended in the atmosphere. Graupel which is able to fall to 4 km, quickly melts in a narrow melting layer.

Hail (Figure 3c) forms either when large rain drops freeze or from a reclassification of graupel when the "wet-growth" regime is reached. As for graupel, hail mass mainly comes from riming, but the location is different from riming onto graupel. Due to slight rotation within the updraft, hail embryos are produced by freezing large raindrops on the eastern side of the updraft (where the largest raindrops are (not shown)). These embryos are then

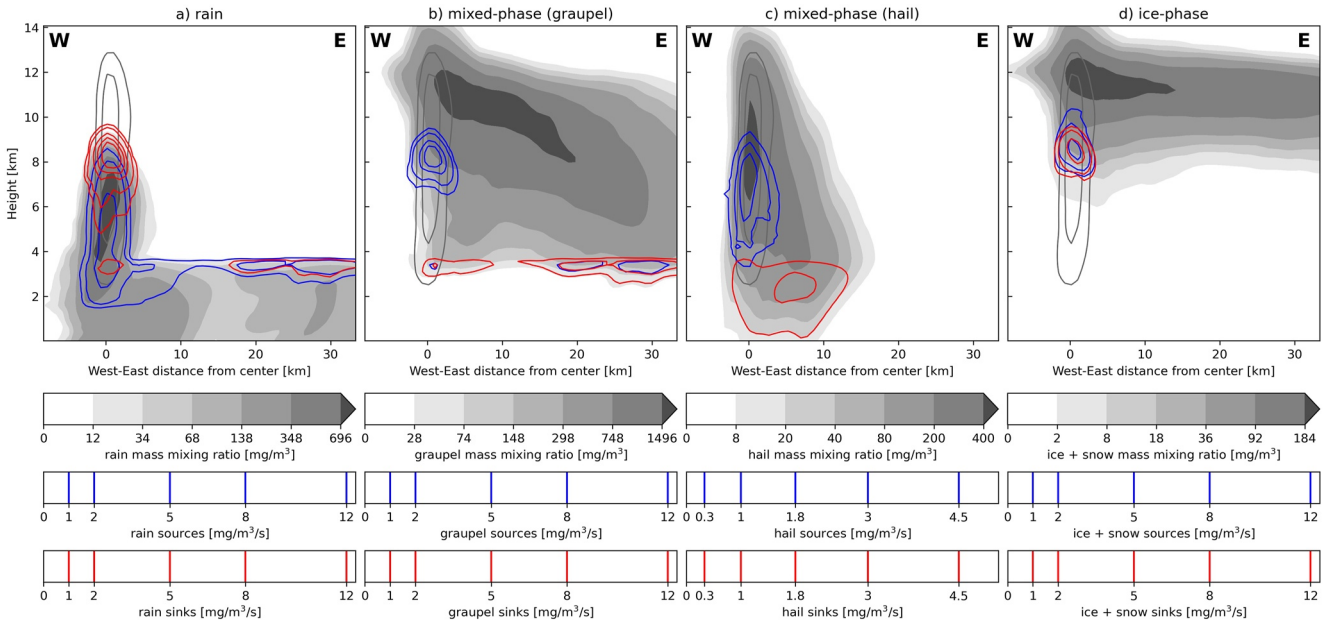

Figure 3. West-East cross-sections (along the mean horizontal wind) through the convective cell in the WS18 + CCN100 simulation showing the relative locations of hydrometeor mass (gray shading), sources of mass (blue contours) and sinks of mass (red contours) for four different hydrometeor categories (a) rain, (b) graupel, (c) hail, and (d) ice and snow combined. Composites are built using values at 5-min intervals between 45 and 90 min simulation time, centered on the cell maximum updraft location at 5 km altitude. Black contour lines are updraft velocities of 10 and 20 m/s. Contour line intervals for the sources and sinks are given one the scales below the plots.

transported from east to west across the updraft, with most of the riming occurring on the western side of the updraft (where the hail embryos have grown larger and the rain mass is most concentrated). Hail riming occurs either at the same altitude and lower than graupel riming. The largest hail stones fall more quickly than graupel and can reach the melting level in the vicinity of the updraft core. Smaller hail stones are continually lifted by the updraft above the region where riming is possible, limiting their growth. These small hail stones fall more quickly than graupel particles and therefore remain much closer to the updraft core than graupel. A broad and deep region of hail melting is present below the melting level, extending to the ground. Some of the largest hail stones are able to reach the surface without fully melting.

Ice and snow are produced through freezing of cloud and rain drops within the updraft at 8–9 km altitude (Figure 3d). Many of these particles are quickly involved in riming and become graupel, hence the co-located source and sink regions. Ice and snow particles which do not become graupel remain small and suspended in the atmosphere above 8 km, moving into the anvil region of the cell and being advected downwind. Ice and snow do not fall to the melting level and are therefore not involved in surface precipitation formation in this simulation.

Simulations with increased wind shear (not shown) produce more tilted and wider updrafts. This allows rain drops to grow via collision and coalescence for a longer time before either reaching the freezing temperatures or moving out of the updraft region.

In simulations with increased CCN concentration (not shown), the collision and coalescence process occurs more slowly. Therefore, the large rain drops needed for freezing are produced later and at higher altitudes. Consequently, less heterogeneous freezing and riming occurs within an air parcel rising through the updraft, allowing more freezing to ice and snow when homogeneous freezing begins at around −38°C. and more ice and snow remains suspended in the atmosphere through the simulation.

The microphysical pathways, and the sensitivity to both CCN and wind shear, are evaluated in more detail in the following section.

3.3. Microphysical Pathways in Model Simulations

The importance of each microphysical pathway is calculated using high time-resolution model output of hydrometeor contents and microphysical process rates. This allows us to almost fully close the hydrometeor mass

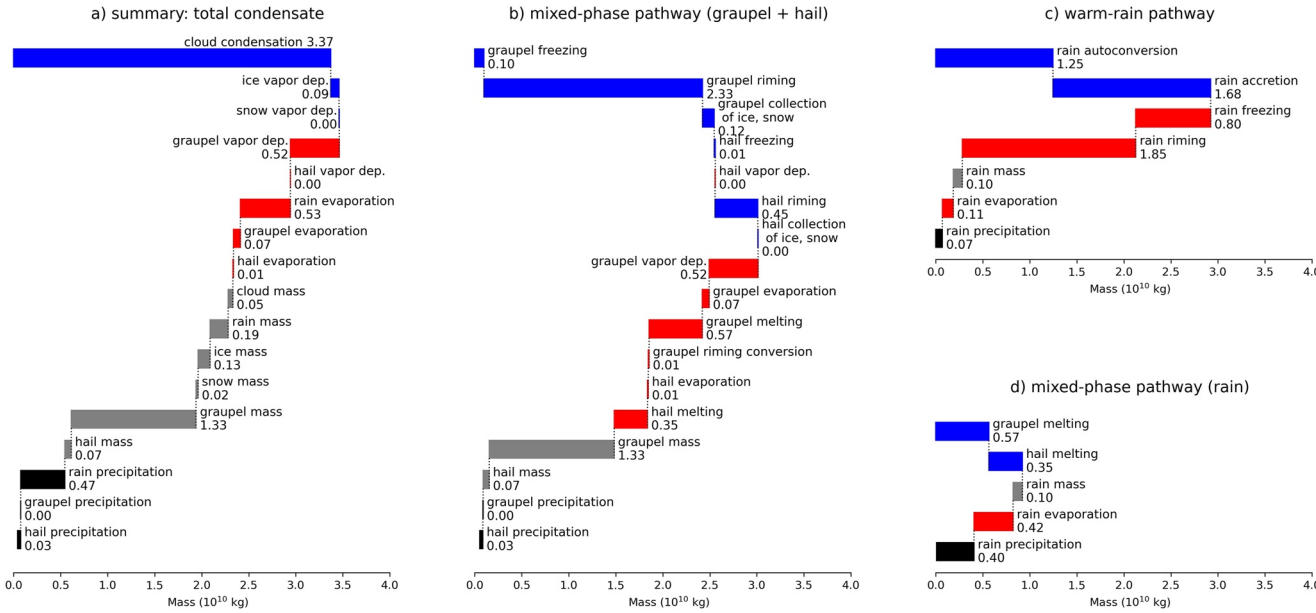

Figure 4. Waterfall charts showing process rates which contribute to the different microphysical pathways. Values are for the WS18 + CCN100 simulation and show whole domain integrals (time and height) for the 2-hr simulation period. Blue represents sources of hydrometeor mass in each pathway and red represents sinks of mass, gray represents mass of hydrometeors in the atmosphere and black represents surface precipitation. Note: graupel vapor deposition is shown as a source, but the net process rate is negative indicating that sublimation is more important than vapor deposition.

budget for each hydrometeor class individually (not shown). Process rates are combined following the possible microphysical pathways, and are displayed as so-called waterfall charts in Figure 4. Waterfall charts visualize the cumulative effects of positive and negative contributions, in this case of the integrated process rates, to the mass budget. We are again able to close the mass budget overall (Figure 4a) and for individual pathways (Figures 4b–4d). This is shown and discussed exemplarily for the WS18 + CCN100 case. In this simulation, hydrometeor mass is formed mainly through condensation (97%, Figure 4a), with a small additional contribution from vapor deposition onto ice (3%). Around 15% of mass is lost via sublimation of graupel (negative vapor deposition), and another 15% from evaporation below the melting level. 0.50×10^{10} kg fell to the surface as precipitation leaving 1.29×10^{10} kg suspended in the atmosphere, mostly as graupel. This equates to a precipitation efficiency (precipitation/condensation) of 14.5% (0.50×10^{10} kg/3.46×10^{10} kg) in this two-hour period.

The microphysical pathway analysis allows to attribute the surface precipitation to either warm-rain or mixed-phase pathways; the ice-phase does not contribute to surface precipitation in these simulations. The mixed-phase pathway produces at least 86% of the surface precipitation (0.03×10^{10} kg hail (Figure 4b) +0.40×10^{10} kg rain from melted graupel and hail (Figure 4d), from 0.50×10^{10} kg total precipitation). This relative contribution from the mixed-phase pathway is likely an underestimate, as discussed below, and therefore the warm-rain pathway (Figure 4c) barely contributes at all to surface precipitation. Rain water mass produced by autoconversion and accretion of cloud water is almost completely removed by freezing and riming before it can fall out of the updraft.

In contrast, rain formed through melting of graupel and hail produces almost all of the surface precipitation (Figure 4d). With the assumed initial moisture profile of 100% at the surface and slightly above 80% at cloud base (Weisman & Klemp, 1982), almost half of all rain water from melting evaporates before reaching the ground. An equivalent amount reaches the ground as rain, with roughly 10% still falling from the cloud at the end of the simulation. More than 90% of the graupel and hail mass is produced by riming (Figure 4b), with small contributions from the freezing of rain drops and the formation of graupel embryos, which originally grew as ice or snow. Around half of the graupel mass produced during the simulation remains suspended in the atmosphere at the end, whereas the remaining more than 50% of the graupel and hail mass melts to become rain (Figures 4b and 4d). Of the 0.45×10^{10} kg hail mass produced during the simulation, 0.03×10^{10} kg reaches the surface while still solid, 0.07×10^{10} kg is still falling, 0.35×10^{10} kg melts to rain and 0.01×10^{10} kg evaporates (Figure 4b).

Analyzing the microphysical pathways for all simulations shows that the largest contribution to surface precipitation always comes from the mixed-phase pathway (Figure 5). The mixed-phase contribution to surface

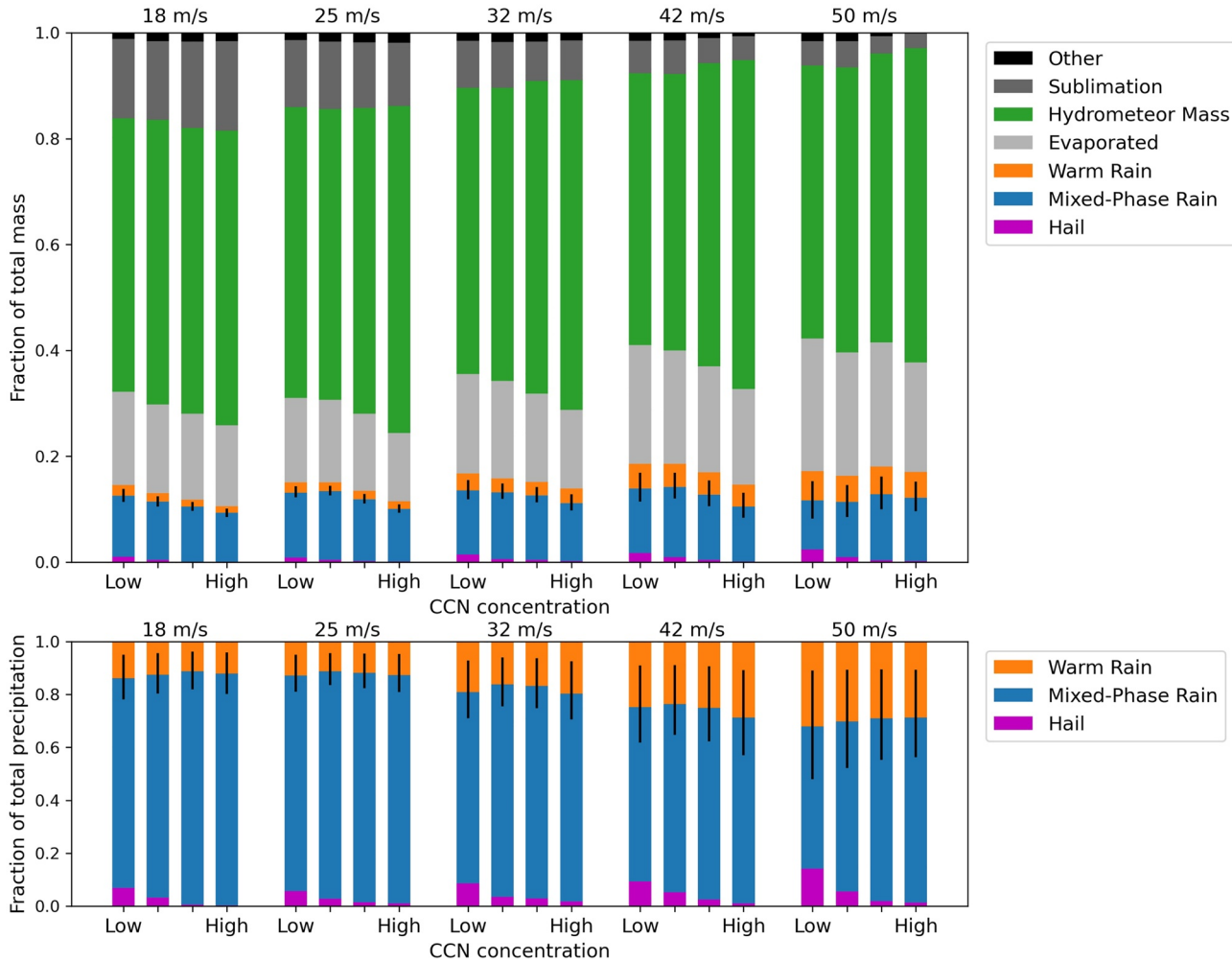

Figure 5. Summary of hydrometeor destinations from each microphysical pathway, including hydrometeors still suspended at the end of the simulation period (green bars) for each simulation. Upper panel shows mass proportional to total condensation whereas lower panel shows mass proportional to total precipitation. Surface rain is attributed to warm and mixed-phase pathways proportional to the total sources and sinks. The error bar for warm and mixed-phase rain shows sensitivity to a factor of 5 change in assumptions about this distribution, see text for more details.

precipitation (the sum of warm rain, mixed-phase rain and hail) increases slightly as CCN concentration is increased. As wind shear is increased the precipitation fraction from the mixed-phase pathway decreases and becomes more uncertain. It is even possible that all surface precipitation comes from the mixed-phase pathway in all simulations. The uncertainty related to this contribution are discussed in the following.

From the analysis of simulation WS18 + CCN100 we conclude that at least 86% of surface precipitation results from the formation (and later melting) of frozen hydrometeors (mainly graupel and hail). However, there is some ambiguity about how to allocate the rain mass in the atmosphere, rain evaporation and surface precipitation among the warm and mixed-phase pathways. We allocate them as follows. Rain mass above the melting level is warm rain (although it might later freeze or rime, and therefore contribute to the mixed-phase pathway). Rain mass below the melting level, total evaporation and surface precipitation are allocated to both warm and mixed-phase pathways such that the ratio of these 3 values is the same for each pathway. This assumes that evaporation of warm rain and mixed-phase rain is equal. This assumption is poor. Melted graupel and hail stones produce larger rain hydrometeors than those formed through warm rain processes. Therefore warm rain would evaporate more quickly than mixed-phase rain, meaning that the 86% estimate from the mixed-phase pathway would be an underestimate. To quantify these uncertainties, the separation was again performed with mass:precipitation:evaporation ratios of 1:1:5 (warm rain evaporates faster) and 5:5:1 (warm rain evaporates slower). These values are shown by the black error bars in Figure 5. For all cases, the mixed-phase pathway is more

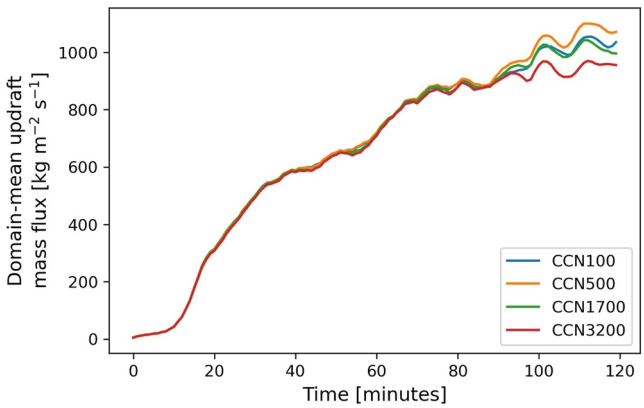

Figure 6. Timeseries of total integrated upward mass flux from all WS18 simulations. Lines are colored by their respective cloud condensation nuclei concentration.

important than the warm rain pathway. The relative importance of the warm rain pathway increases with increasing wind shear, as does the uncertainty. However, it is possible and plausible that all surface precipitation originates from the mixed-phase pathway; analysis of the timing and location of surface precipitation and rain evaporation show very strong associations with the timing and location of melting and much lower correlations with autoconversion and accretion processes.

4. Analysis of Sensitivity in the Riming Rate

Riming appears to be the main source of mass for hydrometeors that subsequently reach the ground. It is shown in the previous section that riming contributes more than 90% to the graupel and hail mass (Figure 4b). As the mixed-phase pathway is dominant, the amount of riming therefore determines how much precipitation reaches the ground. There are several possible explanations as to why the riming rate is sensitive to CCN concentration, including: (a) storm updraft size or intensity, (b) amount of available supercooled liquid water, (c) size and concentration of cloud and rain droplets, (d) size and concentration of the graupel and hail. In this section, we attempt to attribute which of these are responsible for the changes of riming rate induced by changing the CCN concentration in the simulations.

4.1. Changes to Updraft Characteristics

It is possible that the updraft characteristics changed due to increased CCN concentrations. Feedbacks through changed latent heating from condensation or freezing, cloud edge evaporation, and additional mass of condensed hydrometeors could all potentially change the buoyancy and/or size of the updraft. Additionally, changes to the cold pool properties via below-cloud evaporation rates can also influence the updraft.

The total upward mass flux (Figure 6), histograms of updraft strength (not shown) and profiles of integrated condensation rate (not shown), each show only small changes. Total mass flux is almost unchanged throughout the first 90 min of the simulation. Thereafter, feedbacks begin to affect the updrafts leading to an approximate 10% difference in the upward mass flux after 2 hr. There is no evidence of systematic effects of CCN on the simulated updrafts as would be seen if convective invigoration was occurring.

The changes to surface precipitation are much larger than 10% and occur before 90 min simulation time. Therefore, we conclude that updraft changes cannot be of primary importance for surface precipitation sensitivities in these simulations.

4.2. Availability of Supercooled Liquid Water

Supercooled water is a pre-requisite for the riming process. With all else being equal, riming rate increases linearly with supercooled liquid water content (SLWC; cloud plus rain water mass above the freezing level). Increased CCN results in more cloud droplets, with smaller average sizes. These smaller sized droplets collide with each other less often, so the production of rain-drop-sized particles is slower. We therefore expect a difference in the cloud and rain water contents inside the cloud.

Vertical profiles of these quantities do indeed show that cloud water mass increases with increasing CCN; however, the rain water category decreases an approximately equal amount. Despite the fact that rain droplets fall faster than cloud drops, the difference in SLWC caused by CCN concentration changes is minor (Figure 7 top row).

The vertical profiles of riming rates for hail collecting cloud water and rain water (Figure 7 bottom row) decrease substantially as CCN is increased. These decreases cannot be simply explained by the small changes of supercooled cloud water and rain water mass in the storm. Furthermore, the riming of rain water onto hail is a factor of 3–4 more important than the riming of cloud water onto hail. The reasons for this behavior relate to drop sizes and collection efficiencies and are explored in Section 4.3.

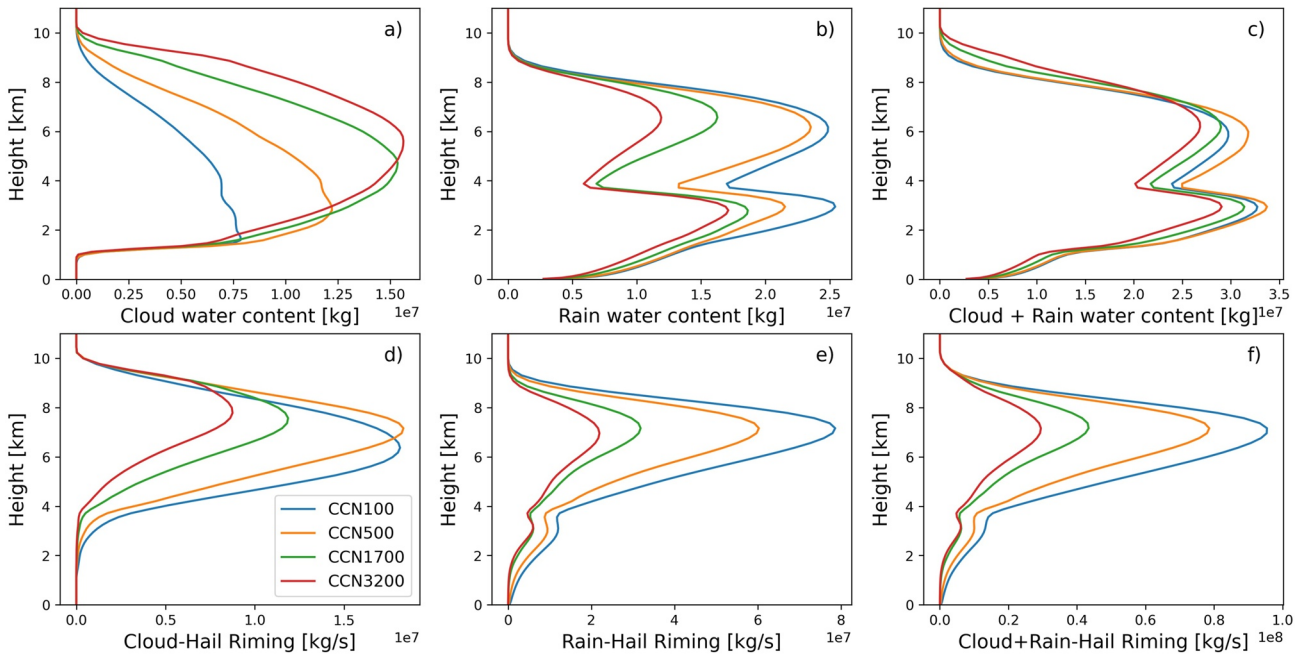

Figure 7. Vertical profiles of simulation-averaged domain-total cloud liquid hydrometeor contents (top row) in kg and time-averaged hail riming rates (bottom row) in kg/s. The WS18 simulations are plotted. Each line represents a different cloud condensation nuclei concentration. Plots for other wind shear simulations are qualitatively similar. The 0°C level is at 4 km altitude.

Previous studies (e.g., Khain et al., 2011 have hypothesized that more SLWC is present in high-CCN environments because the droplets are smaller, take longer to form large rain drop sizes and fall from the cloud and can therefore be transported higher into the cloud. However, our simulations show only a weak sensitivity of SLWC to CCN concentration. The maximum height of SLWC does increase with increasing CCN, driven by changes in cloud water, and this does lead to an increase in riming (especially riming of cloud droplets) at these heights. However, the sensitivity of riming to CCN occurs at lower altitudes (between 4 and 8 km) and is not related to increased SLWC.

Based on these data, we conclude that differences in SLWC cannot be the main cause of the differences in riming rates in our simulations.

4.3. Size-Dependent Riming Efficiency

The size of cloud and rain drops is important because it determines how likely they are to be involved in collisions with other hydrometeors. This is described in the model using the riming efficiency. Smaller droplets have less mass and therefore less inertia. These smaller droplets are more likely to follow the air motion around larger falling graupel or hail particles and avoid a collision, whereas for larger droplets the likelihood of collision is larger. The riming efficiency quantifies both the probability of collision and the probability that the liquid drop and riming particle combine after the collision. Riming efficiency is highest for larger liquid drops.

Cloud droplets are larger under low-CCN conditions. The riming collection efficiency for cloud droplets is parameterized as a linearly increasing function of x_c ($=q_c/n_c$; the mean mass of cloud water drops within the grid box) (Seifert & Beheng, 2006a) and is plotted with a black line in Figure 8. Histograms of grid-box mean cloud droplet size (only at locations where riming is occurring) for simulations with different CCN concentrations are also plotted. Equivalent plots for other wind shear values are almost identical and therefore omitted. The mean riming efficiency of cloud droplets for the CCN100 simulations is around 0.787, which reduces to 0.238 for the CCN3200 simulations. Rain drops are assumed to have a collection efficiency of unity and there is also increased rain water mass and less cloud water in the low-CCN simulations (Figures 7a and 7b) further increasing the sensitivity. Therefore there are two reasons to expect decreased riming rate through decreased riming efficiency as CCN is increased.

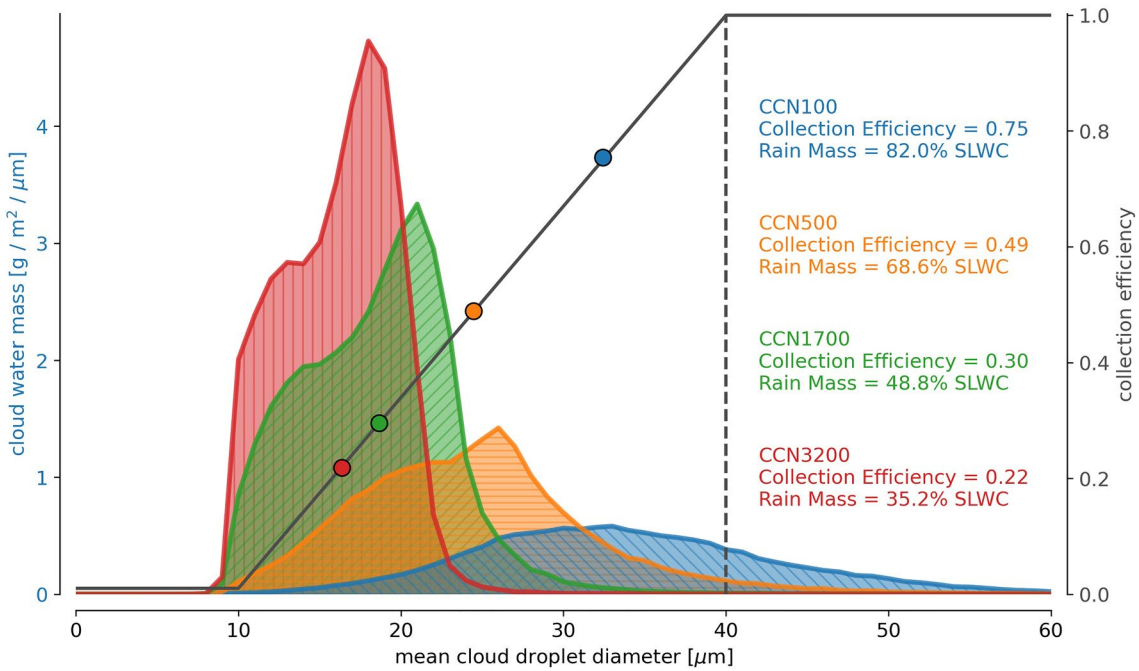

Figure 8. Parameterized riming efficiency (E_{coll}; black line, right axis) plotted with mass-weighted histograms of the grid-box mean cloud water size distribution. Only sub-freezing grid points where riming of cloud water is occurring are included in the histograms. The histograms are plotted for the four different cloud condensation nuclei concentrations. The mean riming efficiency is plotted along the black line with corresponding color and quantified on the right of the plot. The percentage of supercooled water mass in the rain category is also quantified. Plots for all wind shears look similar, so only one (WS18) is shown.

It is hard to theoretically estimate the effect of changing cloud drop riming efficiency on the total riming rate and hence surface precipitation. This is because the riming rate of a hail stone is related to its size. The rate of mass growth therefore increases exponentially over time. Hail particles with a larger initial size, or which can grow rapidly during the early stages of growth, are able to grow relatively faster later in the growth cycle. We cannot easily calculate the importance of these effects for a population of hydrometeors in a complex 3D environment such as these simulated storms. We have therefore performed additional simulations where the riming efficiency of cloud drops is set to constant values of 0.5 and 1.0. $E_{coll} = 0.5$ is an approximate average of riming efficiency across all CCN concentrations. $E_{coll} = 1.0$ is chosen so that there was no difference between the riming efficiency of rain and cloud hydrometeors.

The total surface precipitation and hail fall is much less sensitive to CCN concentration when the riming efficiency is held constant for all cloud drop sizes. Only the WS42 simulations show a systematic decrease of total precipitation with $E_{coll} = 1.0$ (Figure 9a). For all simulations sets, the sensitivity of precipitation to CCN is substantially reduced in these simulations with constant E_{coll}. The sensitivity of hail fall to CCN concentration is also reduced (Figure 9c). WS18 and WS25 simulations now have very little sensitivity. Hail in WS32 simulations responds in a non-systematic way to increased CCN. However, large sensitivities still exist for WS42 and WS50 simulation. These changes cannot be explained by changes to the storm size, as the totals when normalized by the total condensation rate (Figures 9b and 9d) show largely similar sensitivities.

The much reduced sensitivity of surface precipitation and hail when riming efficiency is held constant leads us to conclude that riming efficiency is the most important factor determining surface precipitation changes to CCN concentration in these simulations. Interestingly, the total precipitation and hail amounts now show some non-systematic behavior when only CCN is increased and furthermore show different sensitivities to CCN concentration when the wind shear is changed; this behavior is explored in the next section.

4.4. Size of Graupel and Hail Particles

The size of the graupel and hail particles is important as it determines their potential to collide with supercooled water droplets. Larger graupel and hail have a larger cross-sectional area and particle fall velocity. Therefore

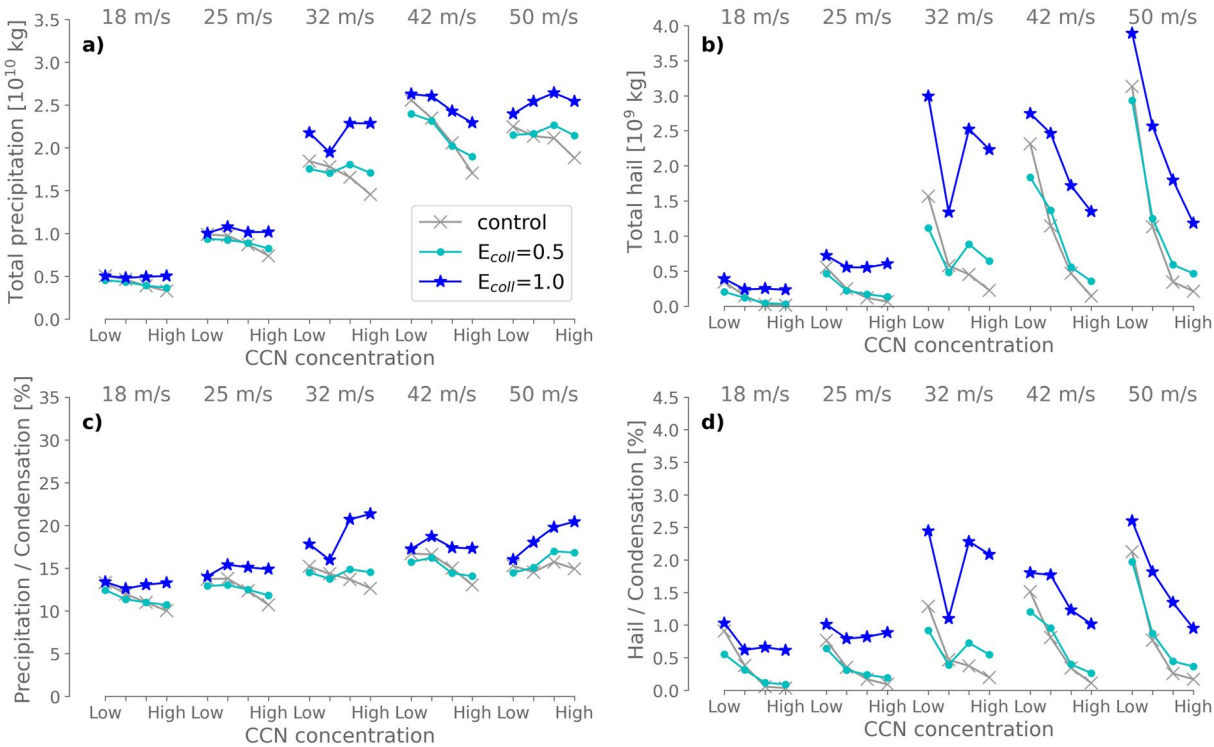

Figure 9. As Figure 1 ("control," gray crosses), but including simulations with E_{coll} of 0.5 (light blue circles) and 1.0 (dark blue stars).

the amount of air "swept out" by the falling hailstone within a given time increases substantially as particle size increases such that larger hail acquires more mass in a given time than small hail.

Furthermore, larger hail is more likely than smaller hail to reach the ground. Because of their larger initial mass and faster fall velocity, large hail stones spend less time falling from the melting level to the ground. As a result, supercooled droplets which rime onto large hail are more likely to reach the surface, and to do so more quickly, than those which rime onto small hail. The total surface precipitation and the storm's precipitation efficiency are both increased by the presence of large hail in the riming region.

Figure 10 shows the distribution of hail stone mass, based on the mass of the grid-box-mean hail stone size and height. Hail size reduces as the CCN concentration increases. In CCN100 simulations, the mass is concentrated toward the largest sizes. The size decreases systematically as the CCN concentration is increased. When averaged over the whole model domain, the average particle mass for hail decreases systematically with increasing CCN concentration (Figure 11a), with only one exception (WS18 + CCN500). Interestingly the mean graupel mass is not so sensitive, and for higher CCN concentrations the mean graupel size is actually larger than the mean hail mass. The changed size distribution results partly from the riming efficiency decreasing with increasing CCN concentration (see previous section). However, similar size distributions are also seen in the constant riming efficiency simulations (Figure 11b).

A more important factor for these differences is the size of hail embryos produced in the simulation. There are two active mechanisms that produce initial hail embryos: freezing of rain drops and conversion of graupel to hail when wet growth begins. The details of these two processes are given in Section 2. Freezing of rain drops is size dependent, and so is the attribution of the frozen rain drops to the ice, graupel and hail categories. In simulations of convective clouds with the Seifert and Beheng (2006a) scheme, the rain drop size generally increases with increasing CCN concentrations, as shown previously (Barthlott & Hoose, 2018). The formation of (smaller) hail embryos by rain freezing produces equal or less mass than the formation of (larger) hail embryos by conversion of graupel for simulations with wind shear up to 32 m/s (Figure 11c). For WS42 and WS50 simulations, the rain freezing process produces more mass and is very sensitive to the CCN concentration: increased CCN concentration leads to increased rain freezing. This is equally true for simulations where $E_{coll} = 1.0$ (Figure 11d).

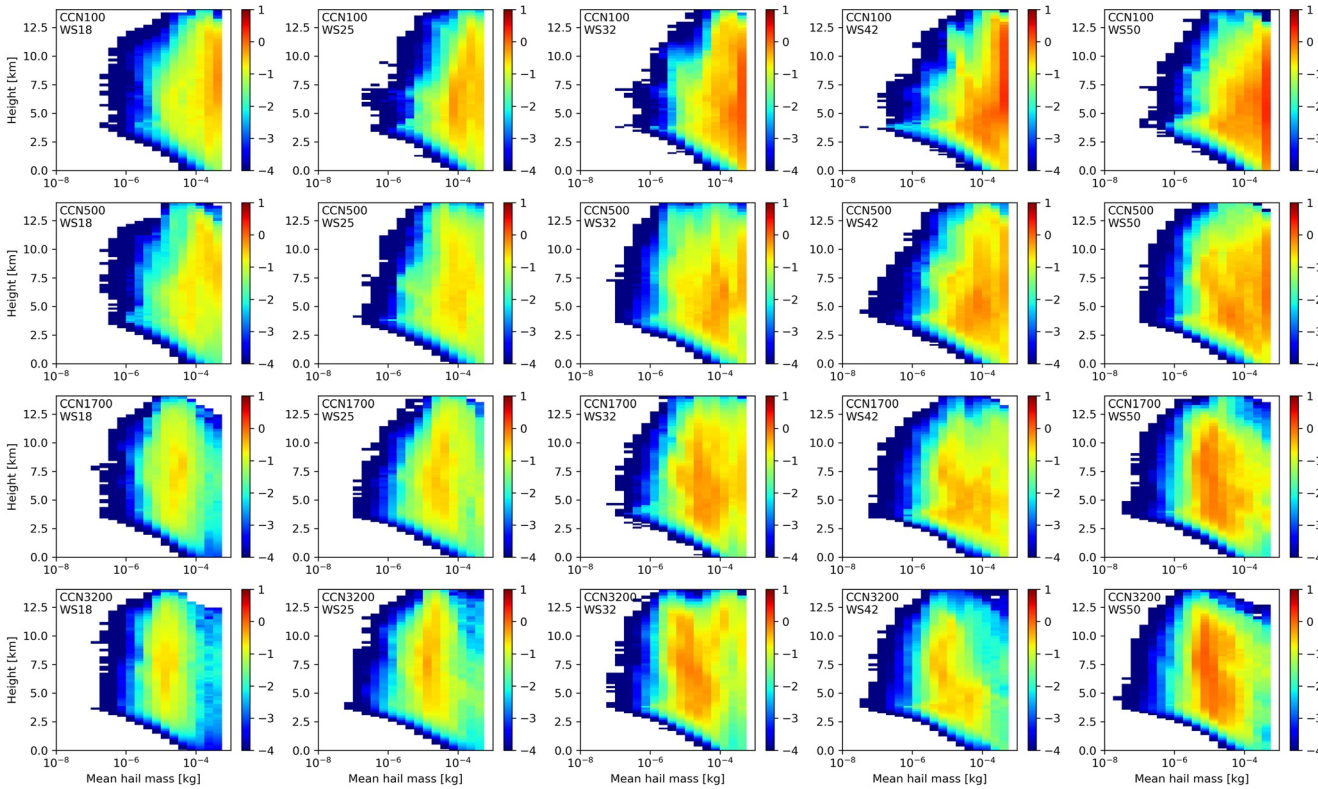

Figure 10. Total hail mass as a function of height and grid-box mean hail stone mass (q_h/n_h). Each row shows simulations with the same cloud condensation nuclei (CCN) concentration (wind shear increasing left to right). Each column shows simulations with the same wind shear (CCN concentration increasing top to bottom). Each color pixel shows $\log_{10}(m)$, where m is total mass in kg.

There is a strong link between the mean size of hail in the simulations and the formation mechanism. Large hail sizes are seen in simulations where wet growth of graupel is the primary mechanism. Smaller sizes occur when rain freezing is the primary mechanism. Smaller hail is more likely to melt fully when falling, therefore the total hail fall is substantially reduced in simulations where only small hail is produced (the high-CCN simulations). A negative correlation is found between total surface hail (Figure 1b) and the rate of hail formation by rain freezing (Figure 11c). The correlation is especially clear when the collection efficiency is set to unity (Figures 9b and 11d) and most obvious when more hail is formed from rain freezing than by graupel undergoing wet growth.

4.5. Summary on Hail Sensitivity to CCN

Summarizing the results of the analyses in Sections 4.1–4.4, increased riming rates for graupel and hail are observed with decreasing CCN concentration, but this does not result from changes in updraft characteristics or changed supercooled liquid water mass in the cloud. Rather, the characteristics of the cloud and rain droplets themselves are important, and in particular their size, which impacts the possible microphysical pathways of hail formation (Figure 12). Lower CCN concentrations therefore produce more hail fall at the surface for the following reasons.

1. Lower CCN concentration means fewer but larger cloud drops. Larger cloud drops have a higher riming efficiency than small cloud drops.
2. Larger cloud drops are more likely to become rain drops. Rain drops have a higher riming efficiency than cloud drops.
3. Lower CCN concentrations result in less rain freezing on average, although this is sometimes a non-systematic signal. Hail embryos formed through conversion of graupel in the wet growth regime produce larger embryos than when formed by freezing of rain drops. Larger hail embryos grow to become larger hail stones which are more likely to reach the surface.

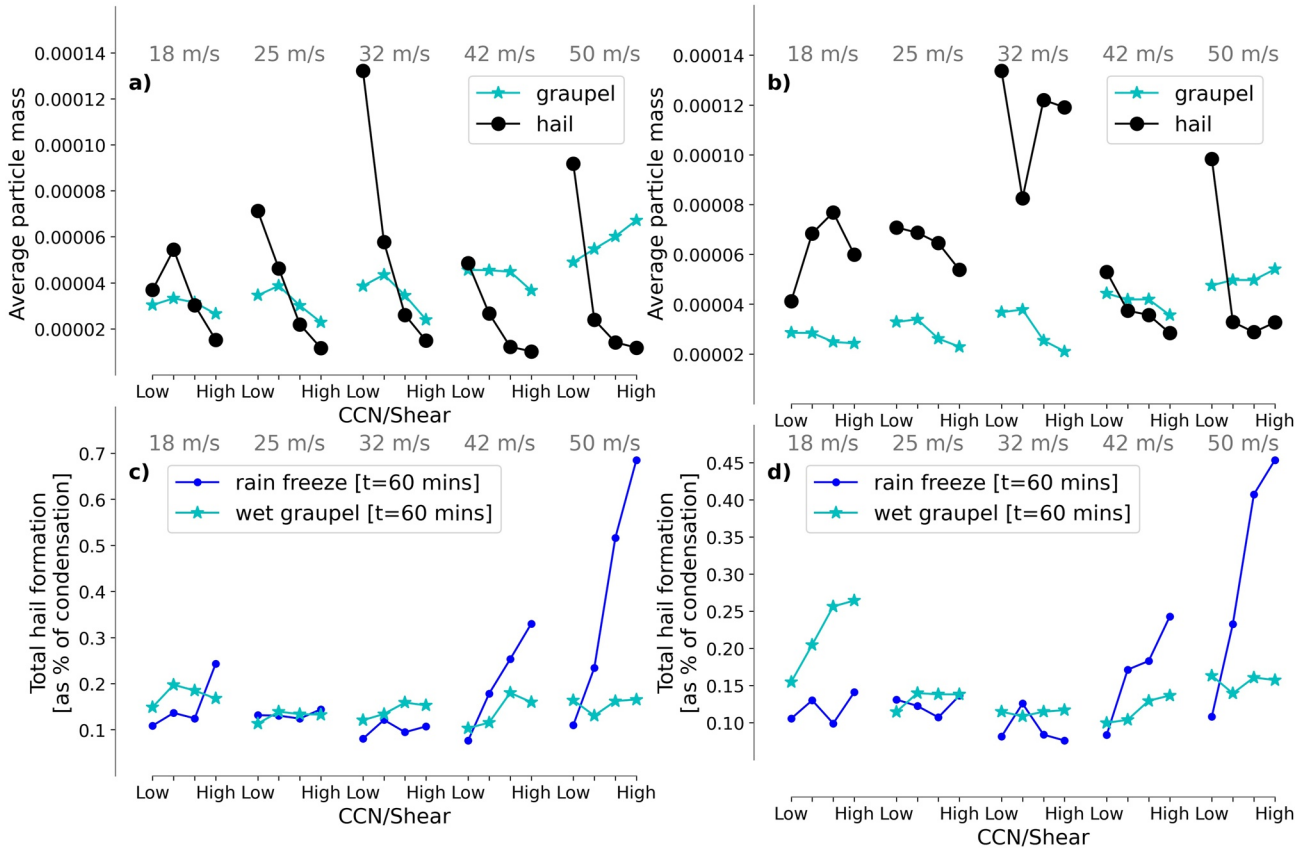

Figure 11. (a) Average particle mass for all graupel and hail particles in each simulation. (b) Average particle mass for all graupel and hail particles for simulations with $E_{coll} = 1.0$. (c) Total mass (normalized by total condensation rate) of hail embryos produced by either rain freezing or conversion of graupel in the wet growth regime. Values are integrated throughout the first 60 min of simulation time. (d) Same for simulations with $E_{coll} = 1.0$.

The change of cloud drop riming efficiency with size is the primary reason for changed surface precipitation totals in these simulations. When the riming efficiency does not change with particle size, the CCN sensitivity of the surface precipitation rate is largely removed. However, the sensitivity of hail fall to CCN still remains for higher wind shear environments (≥32 m/s). These (sometimes non-systematic) changes of hail fall with increasing CCN concentration are explained by changes to hail embryo sizes. Two different mechanisms are responsible for producing hail embryos in the simulation: rain freezing (smaller embryos) and conversion of graupel (larger embryos). Simulations where rain freezing is the most active (typically high wind shear and high CCN concentrations) produce the least surface hail.

5. Discussion

We found that most surface precipitation (whether hail or rain) is formed through the mixed-phase pathway. Riming is the most important process contributing mass in the mixed-phase pathway and we found that the cloud and rain drop size distributions play an important role; larger drop sizes result in faster growth by riming. The availability of large supercooled droplets (whether rain drops or large cloud droplets with high collection efficiency) was important for the formation of large rimed hydrometeors, and it is these large rimed hydrometeors that are responsible for at least two thirds of the surface precipitation. The sensitivity to drop sizes highlights the importance of CCN concentration, even though the contribution of the warm rain pathway to surface precipitation was negligible.

Our results may help to explain the large sensitivity of precipitation in simulations of deep convection to chosen microphysical properties found in previous studies. For example, White et al. (2017) found that swapping between two different microphysics parameterizations, including different autoconversion schemes, affected the simulated

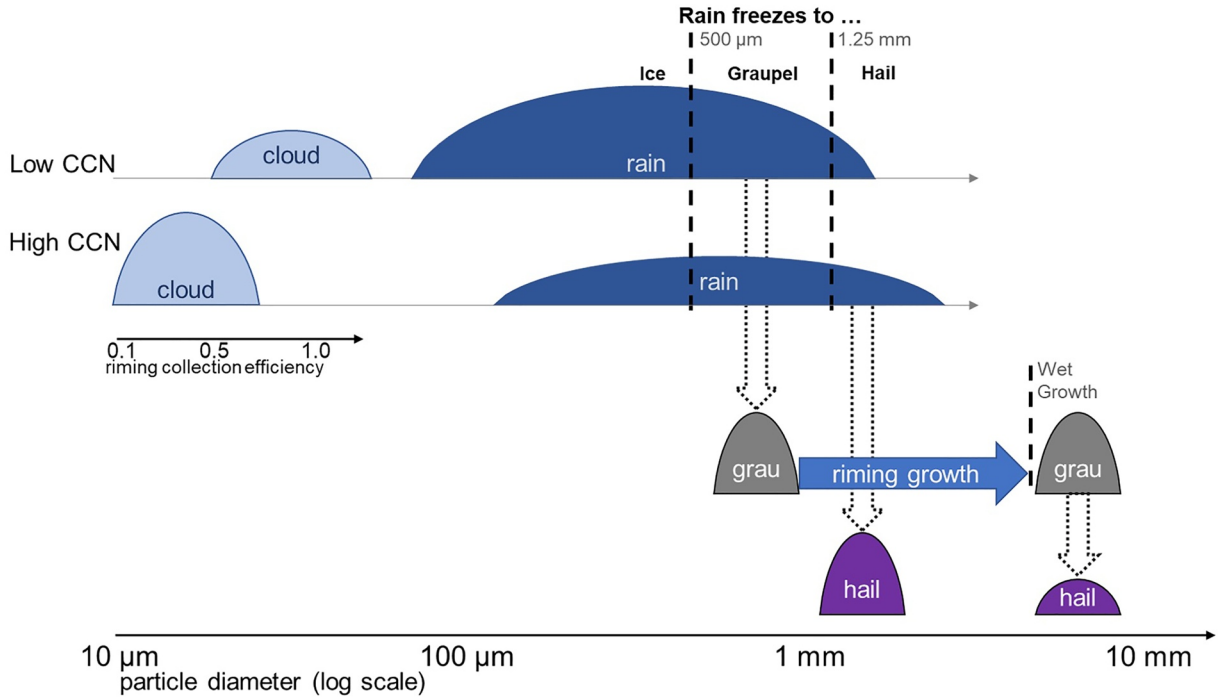

Figure 12. Schematic plot illustrating the two different hail embryo formation pathways. Each semicircle represents an approximate size distribution. Changes of particle class are marked by dotted arrows. Hail formed by rain freezing is much smaller than hail created (in the model) when graupel reaches the wet growth regime. The relative amount of these two hail formation pathways depends on the rain drop size distribution, which in turn is affected by the cloud condensation nuclei concentration.

precipitation from two deep convective cloud cases more than or similarly to changing the CCN concentration did. Therefore, the results of White et al. (2017) may be understood through this mechanism, as the increased availability of large supercooled (rain) hydrometeors should produce additional precipitation. Our analysis of the microphysical pathways gives a new framework for understanding how changes to the warm-rain physics have large impacts on the evolution and precipitation from convective storms. Changes made via changing CCN concentration (as in this study), changing the autoconversion parameterization (as in White et al., 2017) or changing the parameters of the cloud droplet size distribution (such as N_0, μ, ν) (for example, Barthlott et al., 2022) potentially lead to similar physical sensitivities and could be understood consistently. More research comparing these sensitivities is needed.

The sensitivity of surface precipitation and hail to supercooled hydrometeor size is plausible in reality. Our study is limited to analysis of simulated convective cells; however, evidence from radar observations also suggests that large raindrops are present when hail formation occurs. A so-called "differential reflectivity (ZDR) column," a vertically coherent region of increased ZDR values, is often detected in dual-polarimetric observations of convective cells which are producing hail, and the ZDR column depth has been shown to be a good predictor of large hail formation (Ilotoviz et al., 2018; Kumjian et al., 2014; Kuster et al., 2019). Large ZDR values are interpreted as being a signal of large oblate liquid hydrometeors several mm in diameter (such as large rain drops), and have been observed to extend 3 km above the melting level. The presence of the ZDR column can be used for nowcasting hail in the next 10–15 min (Kumjian et al., 2014). It is therefore plausible that the sensitivities and mechanisms relating to riming efficiency discussed in this article apply not only to idealised simulations but also to real convective cells. Nevertheless, more realistic simulations combined with observational evidence are needed to confirm this.

The second important sensitivity, to the process producing hail embryos, is more difficult to link to reality, although early studies have attempted to identify hail embryos and their properties in photographs of hailstone sections (for example, Knight & Knight, 1970]. Reality does not have separate categories for graupel and hail. Therefore whether the diameter of a frozen raindrop exceeds a threshold size does not determine its classification or affect its chance of becoming a large hail stone later. Larger sized frozen drops do grow faster, but their

characteristics (such as density and fall velocity) are determined by the current size not by the initial size at formation. In the model representation, this can only change if a graupel stone enters the wet growth regime and gets reclassified as hail. It is therefore likely that the surface precipitation and potentially the CCN sensitivity depends on the threshold sizes in the rain freezing parameterization. A similar analysis using the Predicted Particle Properties (P3 Morrison & Milbrandt, 2015) microphysics scheme, where particle density can evolve with time, or using particle trajectory calculations (Kumjian & Lombardo, 2020) would both be helpful to check the robustness of these results.

The relatively large sensitivity to CCN concentration could also be interpreted as a consequence of "beneficial" competition between the many, small hail embryos formed by freezing of rain drops. Although the partially arbitrary classification of frozen rain drops as graupel or hail is potentially leading to an artificially strong effect, the importance of beneficial competition among growing hail has been theorised in the context of hail suppression (e. g., Atlas, 1977).

The accuracy of the riming calculations in the model is of importance because the riming process was the most important for producing surface precipitation in these simulations. The representation of riming in the Seifert and Beheng (2006a) scheme is quite detailed, using a collision kernel based on the full particle size distributions of both hydrometeor species involved in each calculated collision type. However, the collision kernel between droplets and ice particles depends on habit and degree of riming, such that available parameterizations give divergent results (Brdar & Seifert, 2018). A simplification in the Seifert and Beheng (2006a) scheme relates to the riming efficiency, which is (a) represented by a linear function of liquid droplet size between two thresholds and (b) uses the grid-box mean particle size rather than integrating over the full size distribution. A representation such as that in the "bin-emulating" approach of Saleeby and Cotton (2008) would be more accurate and the benefit of such representation in ICON should be quantified in a future study.

6. Conclusions

Simulations with the ICON model have been used to identify the chain of processes producing precipitation, referred to here as "microphysical pathways," in idealized thunderstorms. The relative importance of each pathway and their sensitivity to CCN concentration and wind shear have been quantified.

In all simulations, 86%–100% of surface precipitation resulted from the melting of frozen hydrometeors. These hydrometeors followed the mixed-phase pathway, where the main source of mass came from riming. Almost no surface rain was produced via the warm-rain pathway (through collision and coalescence parameterized as autoconversion and accretion). No precipitation occurred as the result of melting of ice or snow (the ice-phase pathway). A substantial fraction ($\geq$50%) of all condensed mass remained in the atmosphere at the end of the simulations (the non-precipitating pathway), mostly as small ice and small graupel, both at high-altitudes.

The mixed-phase pathway remains dominant pathway for all CCN and wind shear setups. However, the overall efficiency of converting condensed mass to surface precipitation is decreased by increased CCN concentration. Increasing wind shear led to increased surface rain and hail in almost all situations but it was distributed over a larger area meaning that the local maxima remained similar.

Further breaking down the mixed-phase pathway, there are two important factors that determine the final precipitation and hail totals: riming efficiency and hail embryo size. The riming efficiency, determined by the size of the liquid droplets in each collision, determines how much precipitation mass reaches the surface. Increased riming efficiencies allow mass to be transferred faster to graupel and hail, leading to larger hydrometeors and increased precipitation totals. Lower CCN concentrations result in larger drop sizes and therefore more precipitation. Hail embryo size is determined by how the embryo is formed. Larger hail embryos (as formed when graupel is reclassified as hail in the model) acquire mass more quickly than smaller embryos (mostly formed through freezing of rain drops). Therefore simulated storms with substantial rain freezing contain many small hail embryos which grow and fall more slowly than larger hail, allowing them to melt fully before reaching the surface.

The riming process, part of the mixed-phase pathway where falling frozen hydrometeors collide with and collect supercooled liquid droplets, was the most important process for producing hydrometeors which contribute to surface precipitation. Although the warm-rain pathway did not contribute to surface precipitation, the warm-phase properties of the cloud (number concentration, 3D distribution and size of cloud and rain drops)

played an important role in the precipitation process - due to the importance of riming. The properties of the liquid drops determine the efficiency at which they are collected by falling frozen hydrometeors, with larger drops more likely to be collected. Therefore, the presence of rain and large cloud drops (≥40 μm) in regions where frozen hydrometeors fall is critical for the amount of surface precipitation produced.

Increasing the CCN concentration produced smaller and more numerous cloud droplets and also affected the size and concentration of rain drops within the cloud, and therefore surface precipitation. The smaller cloud drops slow precipitation production via the mixed-phase pathway in two ways: (a) the smaller cloud drops are collected less efficiently by falling frozen hydrometeors and (b) the cloud drops grow to the size of rain drops more slowly, maintaining their low collection efficiency for longer. Increased CCN concentration therefore leads to an increased mass of hydrometeor mass suspended in the atmosphere and smaller precipitation particles, increasing the chance of melting and/or evaporation before reaching the surface and therefore reducing the surface precipitation and hail totals.

Removing the size dependence of the riming efficiency largely removed the sensitivity of surface precipitation to CCN. However, the surface hail totals still showed sensitivity to CCN concentration in some setups, especially those with high wind shear (≥32 m/s). The remaining sensitivity related to hail embryo size. More hail embryos were formed at high CCN concentrations but they were smaller; the total hail embryo mass was almost constant for all CCN concentrations. The hail stones then grew more slowly, reached smaller maximum sizes and were more likely to melt fully before reaching the surface. As illustrated in Figure 12, the largest hail embryos were produced when graupel became hail as it entered the wet growth regime. Rain freezing produced smaller hail embryos on average. Simulations with large amounts of hail produced by rain freezing (e.g., high CCN concentration) therefore had the smallest hail stones and the least surface hail, even when the riming efficiency did not depend on liquid drop size.

Although the results presented in this paper come only from idealized model simulations, the formation of hail in the presence of large supercooled hydrometeors appears consistent with observations of ZDR columns in radar observations. These columns of positive ZDR are thought to indicate regions of large oblate liquid hydrometeors and are indicative of convective cells likely to produce hail. On the other hand, the model sensitivity of surface precipitation and hail to hail embryo formation mechanism is not currently supported by any observational evidence. The mechanism may be dependent on certain size thresholds defined in the model parameterizations. Further model and observational studies are needed to determine the importance of hail embryo size and their associated formation mechanisms.

As detailed in the introduction, there is currently no consensus in the literature about the sign of the sensitivity of surface precipitation or hail to changed CCN concentrations. Therefore, our results agree with some of the existing literature and disagree with other studies. However, the method presented here to understand the relative sensitivities of different microphysical pathways can be used to determine whether the sensitivities in ICON are consistent for other environmental conditions and can be applied in other models/microphysical parameterizations too. Application of this microphysical pathway analysis to other simulation data sets with diverse responses of precipitation to CCN perturbations may help explain the origin of these differences.

Data Availability Statement

Post-processed data from the model simulations are available in the open access repository KITopen (Barrett & Hoose, 2023). The ICON model source code is available under an institutional or a personal non-commercial research license.

Acknowledgments
The research leading to these results was partly performed within subproject B1 of the Transregional Collaborative Research Center SFB/TRR 165 "Waves to Weather" funded by the German Research Foundation ("Deutsche Forschungsgemeinschaft," DFG). Additional work was performed under the subproject "Evaluating and Improving Convection-Permitting Simulations of the Life Cycle of Convective Storms using Polarimetric Radar Data" (BA 6521/1-1) under the programme SPP-2115 "PROM." CH acknowledges funding from the European Research Council (ERC) under the European Union's Horizon 2020 research and innovation programme under Grant agreement 714062 (ERC Starting Grant "C2Phase"). This work was performed on the computational resource ForHLR II funded by the Ministry of Science, Research and the Arts Baden-Württemberg and DFG. Dr. Bethan White and two anonymous reviewers are gratefully acknowledged for constructive comments which helped to improve this manuscript. Open Access funding enabled and organized by Projekt DEAL.

References

Atlas, D. (1977). The paradox of hail suppression. *Science*, *195*(4274), 139–145. https://doi.org/10.1126/science.195.4274.139

Barrett, A. I., & Hoose, C. (2023). Research data for "microphysical pathways active within thunderstorms and their sensitivity to CCN concentration and wind shear" [Dataset]. KITopen. https://doi.org/10.5445/IR/1000156063

Barrett, A. I., Wellmann, C., Seifert, A., Hoose, C., Vogel, B., & Kunz, M. (2019). One step at a time: How model time step significantly affects convection-permitting simulations. *Journal of Advances in Modeling Earth Systems*, *11*(3), 641–658. https://doi.org/10.1029/2018MS001418

Barthlott, C., & Hoose, C. (2018). Aerosol effects on clouds and precipitation over central Europe in different weather regimes. *Journal of the Atmospheric Sciences*, *75*(12), 4247–4264. https://doi.org/10.1175/JAS-D-18-0110.1

Barthlott, C., Zarboo, A., Matsunobu, T., & Keil, C. (2022). Importance of aerosols and shape of the cloud droplet size distribution for convective clouds and precipitation. *Atmospheric Chemistry and Physics*, *22*(3), 2153–2172. https://doi.org/10.5194/acp-22-2153-2022

Bigg, E. (1953). The formation of atmospheric ice crystals by the freezing of droplets. *Quarterly Journal of the Royal Meteorological Society*, *79*(342), 510–519. https://doi.org/10.1002/qj.49707934207

Blahak, U. (2008). Towards a better representation of high density ice particles in a state-of-the-art two-moment bulk microphysical scheme. In *Proceedings of the 15th international Conference Clouds and precipitation*.

Brdar, S., & Seifert, A. (2018). McSnow: A Monte-Carlo particle model for riming and aggregation of ice particles in a multidimensional microphysical phase space. *Journal of Advances in Modeling Earth Systems*, *10*(1), 187–206. https://doi.org/10.1002/2017MS001167

Carrió, G. G., Cotton, W. R., & Loftus, A. (2014). On the response of hailstorms to enhanced CCN concentrations. *Atmospheric Research*, *143*, 342–350. https://doi.org/10.1016/j.atmosres.2014.03.002

Chen, Q., Yin, Y., Jiang, H., Chu, Z., Xue, L., Shi, R., et al. (2019). The roles of mineral dust as cloud condensation nuclei and ice nuclei during the evolution of a hail storm. *Journal of Geophysical Research: Atmospheres*, *124*(24), 14262–14284. https://doi.org/10.1029/2019jd031403

Grabowski, W. W., & Morrison, H. (2017). Modeling condensation in deep convection. *Journal of the Atmospheric Sciences*, *74*(7), 2247–2267. https://doi.org/10.1175/JAS-D-16-0255.1

Ilotoviz, E., Khain, A., Ryzhkov, A. V., & Snyder, J. C. (2018). Relationship between aerosols, hail microphysics, and ZDR columns. *Journal of the Atmospheric Sciences*, *75*(6), 1755–1781. https://doi.org/10.1175/JAS-D-17-0127.1

Khain, A., Rosenfeld, D., Pokrovsky, A., Blahak, U., & Ryzhkov, A. (2011). The role of CCN in precipitation and hail in a mid-latitude storm as seen in simulations using a spectral (bin) microphysics model in a 2D dynamic frame. *Atmospheric Research*, *99*(1), 129–146. https://doi.org/10.1016/j.atmosres.2010.09.015

Khain, A. P., Beheng, K. D., Heymsfield, A., Korolev, A., Krichak, S. O., Levin, Z., et al. (2015). Representation of microphysical processes in cloud-resolving models: Spectral (bin) microphysics versus bulk parameterization. *Reviews of Geophysics*, *53*(2), 247–322. https://doi.org/10.1002/2014RG000468

Khain, A. P., BenMoshe, N., & Pokrovsky, A. (2008). Factors determining the impact of aerosols on surface precipitation from clouds: An attempt at classification. *Journal of the Atmospheric Sciences*, *65*(6), 1721–1748. https://doi.org/10.1175/2007JAS2515.1

Knight, C. A., & Knight, N. C. (1970). Hailstone embryos. *Journal of the Atmospheric Sciences*, *27*(4), 659–666. https://doi.org/10.1175/1520-0469

Kumjian, M. R., Khain, A. P., Benmoshe, N., Ilotoviz, E., Ryzhkov, A. V., & Phillips, V. T. J. (2014). The anatomy and physics of ZDR columns: Investigating a polarimetric radar signature with a spectral bin microphysical model. *Journal of Applied Meteorology and Climatology*, *53*(7), 1820–1843. https://doi.org/10.1175/JAMC-D-13-0354.1

Kumjian, M. R., & Lombardo, K. (2020). A hail growth trajectory model for exploring the environmental controls on hail size: Model physics and idealized tests. *Journal of the Atmospheric Sciences*, *77*(8), 2765–2791. https://doi.org/10.1175/jas-d-20-0016.1

Kuster, C. M., Snyder, J. C., Schuur, T. J., Lindley, T. T., Heinselman, P. L., Furtado, J. C., et al. (2019). Rapid-update radar observations of ZDR column depth and its use in the warning decision process. *Weather and Forecasting*, *34*(4), 1173–1188. https://doi.org/10.1175/WAF-D-19-0024.1

Lebo, Z. J., Morrison, H., & Seinfeld, J. H. (2012). Are simulated aerosol-induced effects on deep convective clouds strongly dependent on saturation adjustment? *Atmospheric Chemistry and Physics*, *12*(20), 9941–9964. https://doi.org/10.5194/acp-12-9941-2012

Loftus, A., & Cotton, W. (2014). Examination of CCN impacts on hail in a simulated supercell storm with triple-moment hail bulk microphysics. *Atmospheric Research*, *147*, 183–204. https://doi.org/10.1016/j.atmosres.2014.04.017

Marion, G. R., & Trapp, R. J. (2019). The dynamical coupling of convective updrafts, downdrafts, and cold pools in simulated supercell thunderstorms. *Journal of Geophysical Research: Atmospheres*, *124*(2), 664–683. https://doi.org/10.1029/2018JD029055

Morrison, H. (2012). On the robustness of aerosol effects on an idealized supercell storm simulated with a cloud system-resolving model. *Atmospheric Chemistry and Physics*, *12*(16), 7689–7705. https://doi.org/10.5194/acp-12-7689-2012

Morrison, H., & Milbrandt, J. A. (2015). Parameterization of cloud microphysics based on the prediction of bulk ice particle properties. Part 1: Scheme description and idealized tests. *Journal of the Atmospheric Sciences*, *72*(1), 287–311. https://doi.org/10.1175/jas-d-14-0065.1

Noppel, H., Blahak, U., Seifert, A., & Beheng, K. D. (2010). Simulations of a hailstorm and the impact of CCN using an advanced two-moment cloud microphysical scheme. *Atmospheric Research*, *96*(2–3), 286–301. https://doi.org/10.1016/j.atmosres.2009.09.008

Phillips, V. T. J., DeMott, P. J., & Andronache, C. (2008). An empirical parameterization of heterogeneous ice nucleation for multiple chemical species of aerosol. *Journal of the Atmospheric Sciences*, *65*(9), 2757–2783. https://doi.org/10.1175/2007JAS2546.1

Rotunno, R., Klemp, J. B., & Klemp, M. L. (1988). A theory for strong, long-lived squall lines. *Journal of the Atmospheric Sciences*, *45*(3), 463–485. https://doi.org/10.1175/1520-0469

Saleeby, S. M., & Cotton, W. R. (2008). A binned approach to cloud-droplet riming implemented in a bulk microphysics model. *Journal of Applied Meteorology and Climatology*, *47*(2), 694–703. https://doi.org/10.1175/2007jamc1664.1

Segal, Y., & Khain, A. (2006). Dependence of droplet concentration on aerosol conditions in different cloud types: Application to droplet concentration parameterization of aerosol conditions. *Journal of Geophysical Research*, *111*(15), D15204. https://doi.org/10.1029/2005JD006561

Seifert, A., & Beheng, K. D. (2001). A double-moment parameterization for simulating autoconversion, accretion and selfcollection. *Atmospheric Research*, *59–60*, 265–281. https://doi.org/10.1016/S0169-8095(01)00126-0

Seifert, A., & Beheng, K. D. (2006a). A two-moment cloud microphysics parameterization for mixed-phase clouds. Part 1: Model description. *Meteorology and Atmospheric Physics*, *92*(1–2), 45–66. https://doi.org/10.1007/s00703-005-0112-4

Seifert, A., & Beheng, K. D. (2006b). A two-moment cloud microphysics parameterization for mixed-phase clouds. Part 2: Maritime vs. continental deep convective storms. *Meteorology and Atmospheric Physics*, *92*(1–2), 67–82. https://doi.org/10.1007/s00703-005-0113-3

Stevens, B., & Feingold, G. (2009). Untangling aerosol effects on clouds and precipitation in a buffered system. *Nature*, *461*(7264), 607–613. https://doi.org/10.1038/nature08281

Tao, W.-K., Chen, J.-P., Li, Z., Wang, C., & Zhang, C. (2012). Impact of aerosols on convective clouds and precipitation. *Reviews of Geophysics*, *50*(2), RG2001. https://doi.org/10.1029/2011RG000369

Warren, R. A., Richter, H., Ramsay, H. A., Siems, S. T., & Manton, M. J. (2017). Impact of variations in upper-level shear on simulated supercells. *Monthly Weather Review*, *145*(7), 2659–2681. https://doi.org/10.1175/mwr-d-16-0412.1

Weisman, M. L., & Klemp, J. B. (1982). The dependence of numerically simulated convective storms on vertical wind shear and buoyancy. *Monthly Weather Review*, *110*(6), 504–520. https://doi.org/10.1175/1520-0493

Wellmann, C., Barrett, A., Johnson, J., Kunz, M., Vogel, B., Carslaw, K., & Hoose, C. (2018). Using emulators to understand the sensitivity of deep convective clouds and hail to environmental conditions. *Journal of Advances in Modeling Earth Systems*, *10*(12), 3103–3122. https://doi.org/10.1029/2018ms001465

White, B., Gryspeerdt, E., Stier, P., Morrison, H., Thompson, G., & Kipling, Z. (2017). Uncertainty from the choice of microphysics scheme in convection-permitting models significantly exceeds aerosol effects. *Atmospheric Chemistry and Physics*, *17*(19), 12145–12175. https://doi.org/10.5194/acp-17-12145-2017

Zhang, Y., Fan, J., Li, Z., & Rosenfeld, D. (2021). Impacts of cloud microphysics parameterizations on simulated aerosol–cloud interactions for deep convective clouds over Houston. *Atmospheric Chemistry and Physics*, *21*(4), 2363–2381. https://doi.org/10.5194/acp-21-2363-2021